Materials Today Communications 35 (2023) 106286

Contents lists available at ScienceDirect

Materials Today Communications

journal homepage: www.elsevier.com/locate/mtcomm

Oxide derived Cu nanofibril assembly for enhanced nonenzymatic glucose sensing

Baleeswaraiah Muchharla [a], Brianna Barbee [a], Marlon Darby [a], Wei Cao [b], Hani Elsayed–Ali [b], Kishor Kumar Sadasivuni [c], Adetayo Adedeji [d], Kapil Kumar [e], Abdennaceur Karoui [f], Preety Panwar [g,h], Gymama Slaughter [i,*], Bijandra Kumar [a,*]

[a] Department of Mathematics, Computer Science and Engineering Technology, Elizabeth City State University, Elizabeth City, NC 27909, USA
[b] Department of Electrical and Computer Engineering, Old Dominion University, Norfolk, VA 23529, USA
[c] Center for Advanced Materials, Qatar University, 2713 Doha, Qatar
[d] Department of Natural Sciences, Elizabeth City State University, Elizabeth City, NC 27909, USA
[e] Laboratory of Environmental Sustainability and Energy Research (LESER), National Institute of Technology Delhi, New Delhi 110040, India
[f] Center for Research Excellence in Science and Technology (CREST), Department of Mathematics and Physics, North Carolina Central University, Durham, NC 27707, USA
[g] Department of Oral Biological and Medical Sciences, Faculty of Dentistry, University of British Columbia, Vancouver, BC V6T1Z3, Canada
[h] Centre for Blood Research, University of British Columbia, Vancouver, BC V6T 1Z3, Canada
[i] Center for Bioelectronics, Old Dominion University, 4211 Monarch Way, Norfolk, VA 23508, USA

ARTICLE INFO

Keywords:
Glucose detection
Copper nanofibril structure
Nonenzymatic sensor
Nanocatalysts

ABSTRACT

In this report, we have prepared copper nanofibril assembly via thermal oxidation followed by electrochemical reduction processes, exhibiting superior glucose detection ability. The morphological analysis evidenced the formation of rough islands or nanofibril structure on the Cu surface depending on initial thermal oxidation temperature. The glucose detection performance was investigated by performing cyclic voltammetry and chronoamperometry with varying glucose concentration. A high sensitivity (4131.57 μA mM^{-1} cm^{-2}), low detection limit (1.41 μM), wider linear range (0–3.9 mM) and long–term stability (30 days) have been recorded for electrode thermally oxidized at 400 °C followed by electrochemical reduction process (rCu_400). The sensitivity is almost three times higher in comparison to the planner Cu surface. This significantly enhanced glucose sensing ability rCu_400 has been attributed to the nanofibril morphology, origination of Cu (111) facet and formation of a stable oxide layer evidenced by scanning electron microscopy, X-ray diffraction and energy dispersive spectroscopy analysis. Despite higher sensitivity, rCu_400 electrode does not show any response to the chloride ion, dopamine, ascorbic acid and uric acid. These results indicate that the Cu nanofibril structure prepared via simple oxidation/reduction process can be an excellent candidate to be used as an electrode for glucose sensing application.

1. Introduction

Diabetes is causing health issues to more than 400 million people worldwide [1,2]. In this regard, fast and reliable glucose monitoring system plays an important role in controlling its adverse effects on health. Among different type of glucose sensing techniques such as spectrometry, fluorescence, chemiluminescence and electrochemistry, the electrochemical glucose biosensors are more beneficial due to their functionality, reliability, portability, and low cost of fabrication [3,4]. The enzyme (glucose oxidase/glucose dehydrogenase) based electrochemical glucose sensors (enzymatic glucose sensors) have excellent glucose detection ability in terms of sensitivity and reliability [5,6]. However, enzymatic glucose sensors are significantly affected by variation in local pH, temperature, and humidity and faces challenges due to the complexity of sensor fabrication, durability of enzymes, high cost, and reproducibility. The fourth–generation metal–based enzyme–free glucose sensors are primarily dependent on the function of catalysts for glucose oxidation reactions [4,7,8].

Electrode materials that facilitate high electrocatalytic activity for glucose oxidation are vital for nonenzymatic glucose sensors [9–13].

* Corresponding authors.
E-mail addresses: gslaught@odu.edu (G. Slaughter), bkumar@ecsu.edu (B. Kumar).

https://doi.org/10.1016/j.mtcomm.2023.106286
Received 11 March 2023; Received in revised form 8 May 2023; Accepted 22 May 2023
Available online 23 May 2023

Cu–based electrodes have been extensively studied and considered as a primary choice among materials used for glucose sensing [4,8]. The glucose sensing mechanism on Cu–based electrodes is governed by the formation of Cu oxides, mainly CuO and Cu_2O. A naturally formed oxide layer can also boost the glucose oxidation reaction of Cu–based catalysts [14]. The CuO and Cu_2O possess intrinsic p–type semiconductive nature exhibiting an indirect bandgap of 1.2–1.9 eV and a direct band gap between 2.0 and 2.17 eV, respectively [15,16]. The Cu_xO oxidation–reduction potential lies within the range of high and low band energies and thus exhibit excellent catalytic properties for glucose sensing reaction. Various types of Cu/Cu oxides structures such as microstructures (e.g., CuO microflowers, microneedles, microspheres [17], microcubes [18], micropillars [19]), nanostructures (e.g., nanoparticles [20], nanorods [21], nanowires [22,23], nanofibers [24], hollow nanocubes [25], nanospheres [26], nanocomposites), thin films (e.g., nanoporous thin films [27]), micro/nano structures [28] and multi–component electrodes (e.g., CuO/Au [29]) have been extensively studied. To use a free–standing electrode, CuO or Cu_2O have been directly grown on the Cu film.

In this work, we have uncovered the glucose sensing properties of Cu nanofibril electrodes prepared via thermal oxidation and electrochemical reduction process. The oxidation temperature plays critical role in altering the morphology of Cu surface. For instance, Cu oxidized at 200 °C and 300 °C exhibit roughened surface with nano/micro grains. However, a nanofibril structure was formed on the Cu surface when sample was oxidized at 400 °C. We have investigated Cu film oxidized at 400 °C and electrochemically reduced (rCu_400) exhibit significantly enhanced glucose sensing ability in comparison to the pristine Cu. The prepared rCu_400 electrode consisting of nanofibril morphology exhibit high sensitivity (4131.57 μA mM^{-1} cm^{-2}), low detection limit (1.41 μM), wider linear range (0 – 3.9 mM), excellent anti–interference characteristics, and durability. Thus, it can be an excellent candidate for the development of nonenzymatic glucose sensors.

2. Material and methods

2.1. Materials

Cu (thickness – 0.25 mm, purity – 99.9 %) was purchased from Alfa Aesar. D– (+)–glucose ($C_6H_{12}O_6$) was purchased from Sigma Aldrich. Acetone, Phosphoric acid, Sodium hydroxide (NaOH, pellets) purchased from Millipore Corp. Uric acid ($C_5H_4N_4O_3$, 99 %) and dopamine hydrochloride ($C_8H_{11}NO_2$·HCl, 99 %) were purchased from Alfa Aesar. L–ascorbic acid ($C_6H_8O_6$, 99 %) purchased from Acrōs Organics. Potassium chloride (KCl) and sodium chloride (NaCl) were purchased from Fisher Chemical. All reagents were used as received without further purification.

2.2. Electrode preparation

Cu samples were mechanically polished with sandpaper with a gauge number of 1000. Next Cu film was cleaned in acetone solution using sonication method (VWR ultrasonic cleaner, Model-97043-964, operating frequency 35 kHz, RF–Power 90 W, sonicated for five minutes) followed by thoroughly rinsing with DI water and drying with nitrogen gas (N_2 gas purity, 99.9 %). The polished Cu film was chemically cleaned in phosphoric acid solution (85 % w/w). The Cu was used as working electrode and a graphite rode as anode. A + 2.5 V was applied to clean the surface of Cu for 15 min. The Cu surface became smooth and clean. Afterward, Cu was cleaned with DI water (rinsed), acetone (rinsed), isopropanol (rinsed) and DI water (rinsed), respectively. The cleaned Cu samples were dried by N_2 and kept in the box furnace. The temperature of the furnace was increased to 200, 300 and 400 °C with a ramping rate of 12.6 deg/min. Next, the temperature was held for one hour then allowed to cool down to room temperature. The oxidized samples were reduced using electrochemical process as discussed earlier [30,31]. In brief, oxidized Cu film was reduced at −1.6 V versus Ag/AgCl in 0.1 M $KHCO_3$ solution for 20 min (Supplementary Fig. S1). The reduced samples were kept in ambient condition and further used for glucose sensing application. Acronyms used for the prepared electrodes are described in Table 1.

2.3. Material characterization

The Cu films were characterized after oxidation using scanning electron microscopy (SEM) (JEOL JSM-6060LV and JEOL JSM-6010PLUS/LA). The elemental composition was identified using a Thermo Scientific Ultradry EDS detector attached to the SEM. We also perform X–ray diffraction (XRD) analysis using a Rigaku MiniFlex II x–ray diffractometer.

2.4. Glucose sensing experiments

Glucose sensing and other electrochemical properties of the prepared electrodes were investigated by performing cyclic voltammetry (CV), Electrochemical impedance spectroscopy (EIS) and chronoamperometry (CA) experiments using BioLogic SP–200 Potentiostat. In brief, the reduced Cu samples were cut into 1 cm × 1.5 cm and used as the working electrodes. The working electrode was attached to a wafer holder and submerged 1 cm deep into the 0.1 M NaOH electrolyte for electrochemical measurements. The glucose sensing experiments were performed on cleaned Cu (Cu) and reduced Cu (rCu_200, rCu_300 and rCu_400) samples as working electrodes, Ag/AgCl (saturated KCl) as reference electrode, and Pt mesh as the counter electrode in 20 mL of 0.1 M NaOH stirring at 500 rpm at room temperature.

3. Results and discussion

3.1. Characterization of oxide derived Cu electrodes

Fig. 1A displays the schematic with optical images of the sample after each synthesis step. Fig. 1B–G shows the change in the morphologies of Cu after oxidation at different temperatures, i.e., 200 °C (Cu–200) (Fig. 1B), 300 °C (Cu–300) (Fig. 1C) and 400 °C (Cu–400) (Fig. 1D). The surface of pristine Cu is featureless and smooth (Supplementary Fig. S2). When the Cu film was oxidized at 200 °C for 1 h (Cu–200), we observed a slight change in the morphology as some micro planner island (with average thickness). The Cu surface transforms into dense nanoisland and more porous nanofibril structures after oxidation at 300 °C (Cu–300) and 400 °C (Cu–400), respectively. Here it should be noted that Cu can be easily oxidized even at ambient temperature, but the process is slow. It is due to formation of top oxide layer which inhibit further Cu oxidation. Thus, the oxidation process is highly dependent on the temperature and duration of the oxidation process. Oxidation at higher temperatures (e.g., 300 °C and 400 °C) originate faster, and more in–depth Cu oxidation generate more rough and porous structure compared to the sample oxidized at low temperature, e.g. 200 °C

Table 1
Sample descriptions of synthesized electrodes.

S. No.	Acronym	Sample description
1	Cu	Pristine Cu
2	Cu–200	Thermally oxidized at 200 °C for 1 h
3	Cu–300	Thermally oxidized at 300 °C for 1 h
4	Cu–400	Thermally oxidized at 400 °C for 1 h
5	rCu_200	Thermally oxidized at 200 °C for 1 h and electrochemically reduced at −1.6 V vs Ag/AgCl, 0.1 M $KHCO_3$ solution
6	rCu_300	Thermally oxidized at 300 °C for 1 h and electrochemically reduced at −1.6 V vs Ag/AgCl, 0.1 M $KHCO_3$ solution
7	rCu_400	Thermally oxidized at 400 °C for 1 h and electrochemically reduced at −1.6 V vs Ag/AgCl, 0.1 M $KHCO_3$ solution

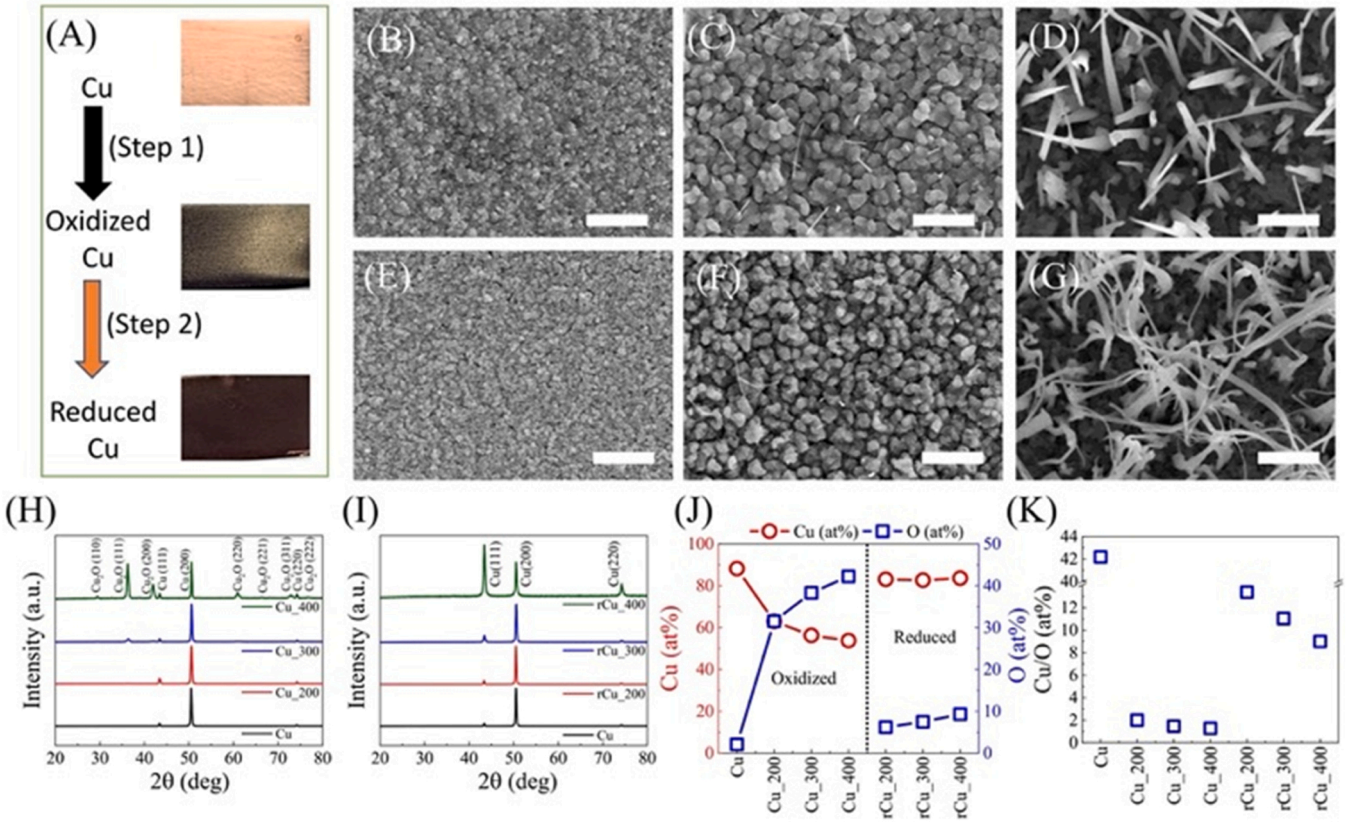

Fig. 1. Physical Characterization of electrodes. (A) electrode preparation steps and corresponding photograph for clean Cu, oxidized Cu (400 °C, 1 h) and after reduction. (B) SEM of Cu oxides at 200 °C (Cu–200), (C) at 300 °C (Cu–300) and (D) at 400 °C (Cu–400). SEM image of reduced sample (E) rCu_200, (F) rCu_300, and (G) rCu_400. The scale bar in B – G is 500 nm. (H) XRD graph for pristine and oxidized Cu, (I) XRD graph for reduced electrodes, (J) Cu and O atomic ratio obtained from EDS analysis and (K) corresponding Cu/O ratio for oxidized and reduced samples.

(Cu–200) [31]. After electrochemically reduction process, the morphologies of samples changes slightly for rCu_200 (Fig. 1E) and rCu_300 (Fig. 1F). However, we have clearly seen the formation of nanofibril structures for samples rCu_400 (Fig. 1G) [30,32].

To understand the change in crystallinity and nature of the samples, we also perform XRD experiments after thermal oxidation and following electrochemical reduction process. The XRD spectra show a new peak ($2\theta = 36°$) for Cu–300 and multiple new peaks for Cu–400 samples (Fig. 1H). These peaks can be associated with the formation of polycrystalline Cu_2O (Fig. 1H). The intensity of polycrystalline Cu_2O increases with oxidation temperature. The XRD spectra of reduced Cu samples i.e., rCu_200, rCu_300, and rCu_400 confirm the absence of any Cu_2O peaks indicating the reduction of Cu_2O into Cu. Interestingly, we have noticed that Cu (111) is the dominated facet for rCu_400 while Cu (200) is the dominant facet for rCu_300, rCu_200, and Cu samples. Next, we performed EDS analysis to visualize the evolution of elemental composition on the surface of electrodes change with the oxidation and the reduction process (Supplementary Fig. S3–S6, Table S1–S7). As displayed in Fig. 1J, the Cu atomic percent (at%) decreases from 88 at% (pristine Cu) to 63 at%, 56 at%, and 53 at% for Cu–200, Cu–300 and Cu–400, respectively. On the other hand, O at% increases from 2 at% to 32 at%, 38 at%, and 42 at% due to thermal oxidation process. These results clearly indicate that with higher oxidation temperature higher Cu_2O forms. After electrochemical reduction process, the Cu at% increases from 63 at% to 83 at% (rCu_200), from 56 at% to 83 at% (rCu_300) and from 53 at% to 84 at% (rCu_400). Similarly, O at% reduced below 10 at% for all samples. The Cu/O ratio decreases from 42 (Cu) to 13 (rCu_200), 11 (rCu_300) and 9 (rCu_400), respectively. These results indicate that even after the reduction, we still have an oxide layer, preferably on the surface of the electrodes.

3.2. Electrocatalysis of glucose at the thermally oxidized/electrochemically reduced Cu samples

3.2.1. Cyclic voltammetry (CV) study

The CVs were collected in 0.1 M NaOH solution without and in the presence of 1 mM glucose by sweeping the potential between –0.6 and 1.0 V with 5 mV/s scan rate (Fig. 2). It should be noted that all potentials are reported with respect to Ag/AgCl (saturated KCl). In NaOH solution, the pristine Cu shows an oxidation peak at 0.0 V followed by a large oxidative tail attributed to the water oxidation after 0.65 V. In the presence of glucose, the intensity of the oxidation peak reduces, and a higher current is observed at higher potential (> 0.5 V) confirming the oxidation of glucose. At 0.65 V, the current density of Cu electrode increases from ~0.08 mA cm^{-2} to ~0.80 mA cm^{-2} after the addition of 1 mM glucose. The mechanism of glucose oxidation at the Cu electrode is well established. In brief, the first step is the formation of Cu oxides (e.g., CuO) due to the adsorption of OH^- ions in NaOH solution (reaction (1)–(3)). The CuO can further interact with OH^- ions making CuOOH as an intermediate active species (reaction (4)–(5)). Here, it should be noted that during this step Cu (II) is converted to Cu (III) which is considered as a catalytic active site responsible for glucose oxidation and gluconolactone formation as a reaction product (reaction (4)). In the last step, glucose to gluconolactone and Cu(III) to Cu(II) conversion occurs simultaneously as shown in reaction (5) [4].

$$Cu \rightarrow Cu^{2+} + 2e^- \quad (1)$$

$$Cu^{2+} + 2OH^- \rightarrow Cu(OH)_2 \quad (2)$$

$$Cu(OH)_2 \rightarrow CuO + H_2O \quad (3)$$

$$CuO + OH^- \rightarrow CuOOH + e^- \quad (4)$$

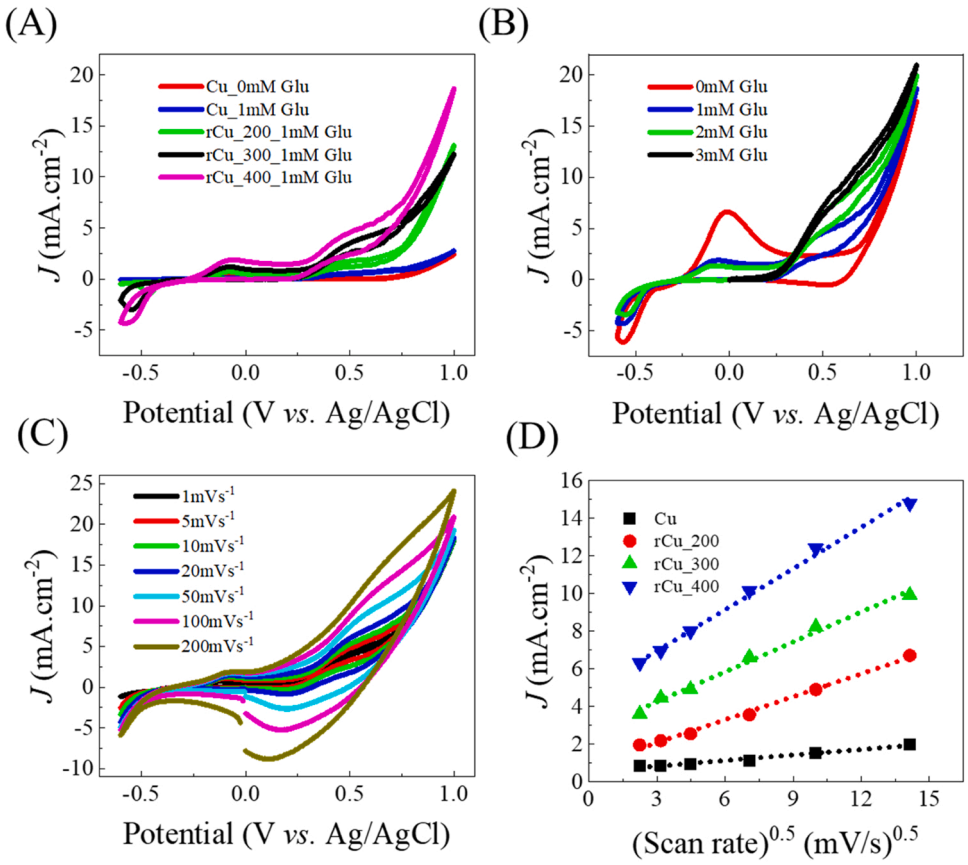

Fig. 2. Glucose sensing characteristic of electrodes. (A) CVs of pristine Cu and reduced electrodes in presence of 1 mM glucose concentration. (B) Effect of glucose concentration on CVs (rCu_400). (C) CVs of rCu_400 electrode at different scan rates from 1 to 200 mV s − 1 in 0.1 M NaOH with 1.0 mM glucose. (D) Glucose oxidation current versus square root of scan rate (v0.5) in 0.1 M NaOH with 1.0 mM glucose.

$$2CuOOH + C_6H_{12}O_6(glucose) \rightarrow 2Cu(OH)_2 + C_6H_{10}O_6\ (gluconolactone) \quad (5)$$

The thermally oxidized/electrochemically reduced Cu electrodes show higher glucose oxidation current in comparison to the pristine Cu. The rCu_200, rCu_300 and rCu_400 exhibit 20.5 (~2.2 mA cm^{-2}), 5.7 (~4.6 mA cm^{-2}), 7.4 (~5.9 mA cm^{-2}) times higher current density at 0.65 V than that of Cu (~0.78 mA cm^{-2}) at the same potential (Fig. 2A). The higher glucose oxidation current densities can be attributed to: (i) an increase in electrochemically active surface area (ECSA) due to a change in the morphology resulting in providing more active sites/cm^2 despite similar geometrical surface area as evidenced by SEM images, and (ii) availability of native Cu oxide (Cu_2O) as evidenced by EDS and formation of Cu (111) facet shown in XRD analysis. It has been previously reported that Cu (111) is relatively more active in comparison to the Cu (100) due to relatively higher electron transport properties [33–35]. This results in improving glucose oxidation reaction kinetics. Moreover, oxide derived Cu consisting of defects such as grain–boundaries, have shown higher intrinsic catalytic activity for other electrochemical reactions such as CO_2 electrochemical conversion processes [30,32]. We also performed CV experiments with varying glucose concentration from 1 to 3 mM, and as expected, with higher concentration of glucose, higher glucose oxidation currents were observed for all examined electrodes (Fig. 2B and Supplementary Fig. S7–S9).

Next, we explored the effect of scan rate on glucose oxidation reaction by performing CV experiments with varying scan rates (1, 5, 10, 20, 50, 100, and 200 mV/s) in the similar potential window (–0.6–1.0 V) and presence of 1.0 mM glucose (Fig. 2C and Supplementary Fig. S10–S12). The anodic peak current density at 0.65 V was selected to plot with respect to the square route of scan rate ($v^{0.5}$) (Fig. 2D). For all the studied electrodes, the results were fitted using the following equation,

$$J\ (mA{\cdot}cm^{-2}) = m(v^{0.5}) + C \quad (6)$$

where J, v, m and C are the current density, scan rate, slope and constant, respectively. We observe good linearity for all electrodes, and rCu_400 shows the highest glucose current density despite different scan rates (Fig. 2D). Based on the linear regression equation analysis, the values of the correlation coefficient (R^2) were 0.982, 0.995, 0.991, and 0.995 for Cu, rCu_200, rCu_300 and rCu_400, respectively. These results clearly indicate that the electrochemical oxidation of glucose is a diffusion–controlled with fast reaction kinetics. Considering the glucose oxidation reaction in the present case as a diffusion–controlled process, a higher magnitude of diffusion coefficient results in higher glucose sensing performance. We further calculated the diffusion coefficient of glucose using Randles–Sevcik equation [36–39] as shown below:

$$I_p = 2.69 \times 10^5 . n^{3/2} . A . D^{1/2} . C . \nu^{1/2} \quad (7)$$

where I_p is the peak current density in amperes, n is the electron transfer number (usually 1), A is the electrode surface geometrical area (in cm^{-2}), C is the bulk concentration (in mol cm^{-3}), v is the scan rate (in V s^{-1}) and D is the diffusion coefficient (cm^2 s^{-1}). Diffusion coefficients were determined from the slopes of I_p versus $v^{0.5}$, for all examined electrodes (Supplementary Table S8). As expected, the magnitude of the diffusion coefficient (1.84 $\times 10^{-5}$ cm^2 s^{-1}) is approximately 54, 3 and 2 times higher compared to the pristine Cu, rCu_200, and rCu_300, respectively.

3.2.2. Chronoamperometry study

The CV analysis provides detailed information about the reaction kinetics while CA is essential to study the applicability of the electrode for glucose sensing application. CA experiments were performed at different operating potentials (i.e., 0.45, 0.65 and 0.75 V) with consecutive addition of 1.0 mM glucose into 0.1 M NaOH at an interval of 60 s (Fig. 3 A, Supplementary Fig. S13–S15). All electrodes exhibit a response even at 0.45 V, but more stable and reproducible signals were recorded at 0.65 V. At higher, potential (0.75 V), we have noticed rapid bubble formation at the counter electrode (Pt) due to water splitting reaction (image is not provided). At every applied potential, rCu_400 exhibited the highest current among all electrodes. We compare the magnitude of the signals collected at 0.65 V by successively adding 1 mM glucose three times. The magnitude of the response i.e., increment in current with the addition of glucose remains almost constant for rCu_400 while it decreases for other electrodes. Mainly, the signal magnitude decreases magnificently with the second and third addition of 1 mM glucose to the Cu and rCu_200 electrodes (Supplementary Fig. S13–S15). For further study, all electrodes were examined at 0.65 V operating potentials.

3.2.3. Sensitivity and limit of detection

The sensitivity, limit of detection (LOD) and linear response for a wide range of glucose concentrations are the key features of glucose sensors. To address these, we performed CA experiments by varying glucose concentration in the range of 5 μM to 10 mM (Fig. 3C, Supplementary Fig. S16–S18). In the case of the rCu_400 electrodes, we noticed very clear signal even for 5 μM glucose concentration (inset of Fig. 3C). Glucose concentration versus current density plot indicates a linear relationship for the lower glucose concentration range of 5 μM to 5 mM. In this range, the LOD was calculated via dividing standard deviation (SD) by the slope of the graph was 1.41 μM for rCu_400. To the opposite, we obtained a relatively higher LOD for Cu (2.43 μM), rCu_200 (2.27 μM), and rCu_300 (1.48 μM) (Table S9). After 5 mM, the magnitude of glucose sensing signal relatively less increased, which can be attributed to the surface saturation of electrodes due to the high density of anion adsorptions. In terms of sensitivity, the rCu_400 electrode exhibits the highest sensitivity (~4131.57 μA mM^{-1} cm^{-2}) among the studied electrodes (Table S9). The LOD and sensitivity of the of Cu–based electrodes are compared in Table 2. The prepared rCu_400 electrodes exhibit competitive glucose sensitivity and LOD despite simple, chemical free fabrication methods. For example, rCu_400 electrode shows ~60 and 20 times lower LOD and ~6 and ~5 times higher sensitivity in comparison to the CuNOx thin film and CuO nanoparticle–based electrodes. In another study, spiky Cu_xO grown on Cu nanowire via electrochemical process have also shown lower sensitivity (1210 μA mM^{-1} cm^{-2}) and relatively poor LOD (10 μM) in comparison to rCu_400 electrode. Moreover, rCu_400 electrode exhibited competitive performance to the Cu/Ni/Au nanoporous film (very high surface area) prepared via electrochemical deposition/magnetron sputtering method [40]. However, a dandelion–like structural electrode shows better performance only in terms of sensitivity (5368.0 μA mM^{-1} cm^{-2}) in comparison to the rCu_400 electrode as it has a very narrow linear detection range (5 – 1.6 mM) (Table 2).

3.2.4. Anti–interference, reproducibility, and stability, of the oxide derived electrodes

The glucose concentration in human blood is more than 30 times higher in comparison to interferences such as uric acid (UA) and others. In blood, the glucose concentration can vary 3–8 mM in normal conditions, while the concentration of interference molecules such as DP (~ 0.1 mM), AA (~ 23 μM), and UA (0.13–0.46 mM) is relatively very low. Thus, we performed interference experiment by successive addition of 1 mM glucose and 0.1 mM interferences (AA, UA, DP, NaCl, KCl) in 0.1 M NaOH solution at 0.65 V (Fig. 4A and Supplementary Fig. S19–S21). The rCu_400 electrode exhibits a well–defined glucose signal (~4.9 mA cm^{-2}) immediately after the addition of 1 mM glucose. However, after the addition of interferences species (0.1 mM), we

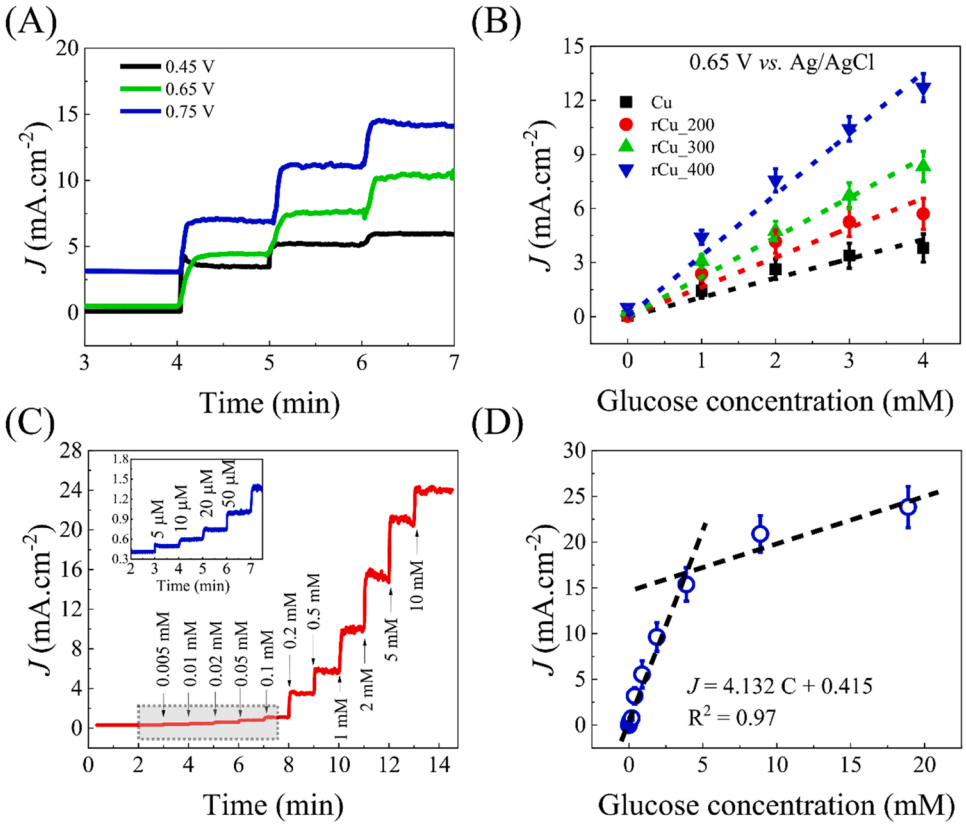

Fig. 3. Amperometry experimental study for prepared electrodes: (A) Amperometry graphs collected at different potential for the rCu_400 film electrode with the successive addition of glucose (0.1 mM) in 0.1 M NaOH, (B) Current density for different electrodes with the successive addition of glucose (0.1 mM) in 0.1 M NaOH at 0.65 V vs Ag/AgCl, (C) response for varying glucose concentration varying from 0.005 to 20 mM and (D) corresponding relative current density with respect to the glucose concentration. The data was fit using linear equation in lower concentration and higher concretion region.

Table 2
Summary of the non–enzymatic electrochemical Cu–based glucose sensors.

Sensing Material	Preparation method	Morphology	LoD (μM)	Sensitivity (μA mM^{-1} cm^{-2})	Linear range (μM–mM)	Ref.
Cu	Wet chemistry	Nanowires	35	420.3	0–3	[41]
Cu/CuO/Cu $(OH)_2$	Chemical method	nanosheets	20	223.17	0–20	[42]
CuO/Cu_2O	Melt spinning/chemical etching	Nanowire	1	1950	100–6	[43]
CuO	hydrothermal method	nanoleaves	0.012	1467.32	5–5.89	[44]
CuO	Solution process	Micro flowers	6.48	10–120	10–0.12	[45]
CuO/Cu	Thermo–chemical method	chrysanthemum–like, candock–like, dandelion–like	0.6, 1.2, 1.2	3251.9 4077.7 5368.0	2–2.3 5–2 5–1.6	[46]
CuO_x/Cu	Electrochemical process	spiky Cu_xO/Cu nanowire	10	1210	10–7	[47]
Cu/Ni/Au	Electrochemical deposition and magnetron sputtering	Nanoporous film	0.1	4135	0.5–3	[40]
Cu_xO/Cu	Chemical oxidation	CuO nanosheets	0.57	1541	0–4	[48]
CuO	Electrospinning and subsequent thermal treatment processes	3D nanofibers	0.8	431.3	6–2.5	[24]
CuO	Electrochemical deposition	Nanoparticles	26	507	0.1–2.5	[49]
CuNOx	Surface Oxidations @RTP	Thin film	94.210	603.420	50.00–7.00	[14]
Cu	Standard sample	Thin film	2.43	1558.12	5–3.88	This work
rCu_200	Thermal oxidation – electrochemical– reduction	Defective oxide thin film	2.27	2560.08	5–3.88	This work
rCu_300	Thermal oxidation – electrochemical–reduction	Nanoclusters	1.48	2877.15	5–3.88	This work
rCu_400	Thermal oxidation – electrochemical– reduction	Nanofibril	1.41	4131.57	5–3.88	This work

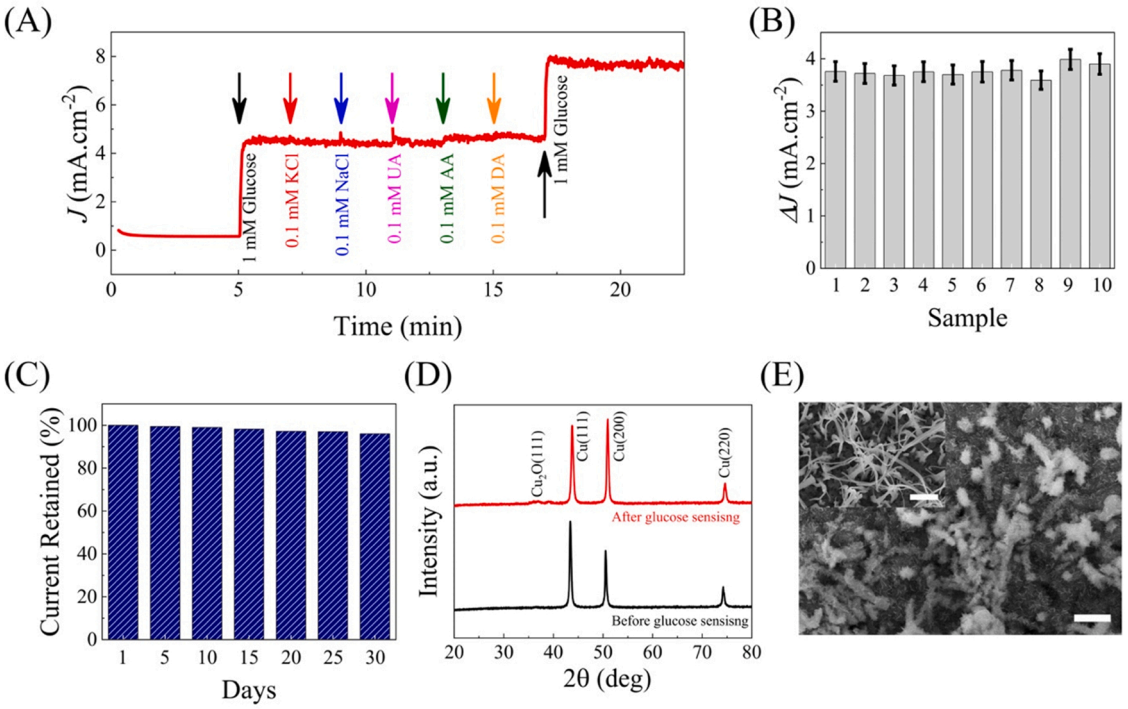

Fig. 4. Interference, stability and reproducibility of the rCu_400 electrode: (A) Response of rCu_400 electrode in presence of interferences KCl, NaCl, AA, DA and UA, (B) response of the rCu_400 electrodes examined at the interval of five days for 30 days and (C) response of the different samples showing the reproducibility of the electrodes. All experiments were performed in 1 mM glucose in 0.1 M NaOH electrolyte. (D) XRD pattern of rCu_400 electrode before (black) and after (red) performing glucose sensing. (E) SEM image of rCu_400 electrode after performing glucose sensing. Inset displays the SEM image of the same electrode before performing glucose sensing. The scale bar is 500 nm.

observed negligible change (few μA.cm^{-2}) in the current. A successive addition of 1 mM.

glucose again shows sharp increment in the current. The results clearly indicate the higher selectivity of the rCu_400 electrodes for the glucose oxidation reaction.

We also tested ten different samples of rCu_400 prepared in three sets, under similar experimental conditions (i.e., 0.65 V, 1 mM glucose, 0.1 M NaOH solution) (Fig. 4B). During these experiments, we observed only 2 % relative standard deviation in the magnitude of the current. We also performed CA experiments using a single electrode within a time-frame of 30 days and recorded results every five days (Fig. 4C). Here it should be noted that rCu_400 electrodes were stored under ambient

conditions and exposed to the environmental condition in the lab. The magnitude of the glucose signal remains almost unchanged and ~98 % current was retained even after 30 days (Fig. 4C). The stability of the rCu_400 electrodes was also determined by performing EIS experiment before and after 30 days (used electrodes). We also performed XRD, SEM and EDS analysis to the rCu_400 electrode examined for long term experiment (30 days). The crystallinity of the rCu_400 electrode slightly changed after glucose sensing experiment, but Cu (111) considered responsible for higher catalytic activity remain unchanged (Fig. 4D). However, we also observed a broad, but small Cu_2O (111) peak indicating the origination of Cu_2O after glucose oxidation experiment and exposure to the ambient conditions (Fig. 4D). Fig. 4E displays SEM image of rCu_400 electrode after performing glucose sensing. Nanofibril structure remains intact, but glucose oxidation developed some needle shaped nanostructures on the nanofibril structure. Based on our SEM and the XRD analysis, these needle shaped nanostructures could be ascribed to newly formed Cu_2O due to experimental process [50]. Similarly, EDS analysis suggest the formation of copper oxides as Cu at% decreased from 84 at% to 55 at% whereas O at% increased from 9 at% to 40 at% (Supplementary Fig. S22 and Table S10). Despite formation of Cu_2O, our EIS analysis suggests a negligible change in charge transfer resistance as the total resistance (~ 6.88 Ω, solution resistance + charge transfer resistance) remain constant (Supplementary Fig. S23). This further confirmed the robustness and stability of the examined electrodes.

4. Conclusions

In conclusion, we have shown that oxide derived Cu exhibits superior glucose sensing ability in comparison to the pristine Cu. The morphology of oxide Cu highly depends on the oxidation temperature and results in nanofibril structure at 400 °C. The rCu_400 electrode preparation method is simple and robust. The high sensitivity of oxide derived Cu electrodes is attributed to the formation of native oxide layer, increase in surface area and formation of Cu (111) facet due to oxidation reduction process. The rCu_400 electrodes exhibit superior anti-–interference characteristics, and it doesn't show any response to 0.1 mM of chloride (KCl and NaCl), UA, DP and AA analytes. The low detection limit (1.41 μM) fast response time (less than second), high sensitivity (4131.57 μA mM^{-1} cm^{-2}), robustness and reproducibly suggest that oxide derived Cu can be an excellent material for practical glucose sensing application.

CRediT authorship contribution statement

Baleeswaraiah Muchharla: Visualization, Conceptualization, Data curation, Formal analysis, Methodology, Validation, Writing - original draft, Writing - review & editing. **Brianna Barbee:** Data acquisition. **Marlon Darby:** Data acquisition. **Kishor Kumar Sadasivuni:** Writing – review & editing. **Adetayo Adedeji:** Writing – review & editing. **Kapil Kumar:** Writing – review & editing. **Abdennaceur Karoui:** Writing – review & editing. **Preety Panwar:** Writing – review & editing. **Gymama Slaughter:** Writing – review & editing. **Bijandra Kumar:** Conceptualization, Methodology, Visualization, Writing – original draft, Supervision, Funding acquisition.

Declaration of Competing Interest

The authors declare that they have no known competing financial interests or personal relationships that could have appeared to influence the work reported in this paper.

Data Availability

Data will be made available on request.

Acknowledgements

Research at the Elizabeth City State University was supported by the Department of Energy- National Nuclear Security Administration (NNSA) grants (DE-NA0003979 and DE-NA0004007).

Author contributions

B.K. and B.M conceived the idea; B.B., M.D. and B.M. prepared the electrodes, performed the electrochemical experiments, collected the results; B.M. and B.K. wrote the first draft; B.K. mentored the B.B., M.D. and B.M. efforts; W.C. and E.H. performed the SEM, XRD and EDS experiment and participated in data analysis; A.A., H.E.A., A.K., K.K.S., P.P. and G.S., participated in analysis of data and support the writing of final draft; All authors have read and approved the article.

Appendix A. Supporting information

Supplementary data associated with this article can be found in the online version at doi:10.1016/j.mtcomm.2023.106286.

References

[1] X. Feng, K. Jiang, S. Fan, M.W. Kanan, A direct grain-boundary-activity correlation for CO electroreduction on Cu nanoparticles, ACS Cent. Sci. 2 (2016) 169–174.
[2] H. Zafar, A. Channa, V. Jeoti, G.M. Stojanović, Comprehensive review on wearable sweat-glucose sensors for continuous glucose monitoring, Sensors 22 (2022).
[3] D.-W. Hwang, S. Lee, M. Seo, T.D. Chung, Recent advances in electrochemical non-enzymatic glucose sensors – a review, Anal. Chim. Acta 1033 (2018) 1–34.
[4] G.A. Naikoo, T. Awan, H. Salim, F. Arshad, I.U. Hassan, M.Z. Pedram, W. Ahmed, H.L. Faruck, A.A.A. Aljabali, V. Mishra, Á. Serrano-Aroca, R. Goyal, P. Negi, M. Birkett, M.M. Nasef, N.B. Charbe, H.A. Bakshi, M.M. Tambuwala, Fourth-generation glucose sensors composed of copper nanostructures for diabetes management: a critical review, Bioeng. Transl. Med. 7 (2022), e10248.
[5] M.H. Hassan, C. Vyas, B. Grieve, P. Bartolo, Recent advances in enzymatic and non-enzymatic electrochemical glucose sensing, Sensors 21 (2021).
[6] M. Zhang, C. Liao, C.H. Mak, P. You, C.L. Mak, F. Yan, Highly sensitive glucose sensors based on enzyme-modified whole-graphene solution-gated transistors, Sci. Rep. 5 (2015) 8311.
[7] W.-C. Lee, K.-B. Kim, N.G. Gurudatt, K.K. Hussain, C.S. Choi, D.-S. Park, Y.-B. Shim, Comparison of enzymatic and non-enzymatic glucose sensors based on hierarchical Au-Ni alloy with conductive polymer, Biosens. Bioelectron. 130 (2019) 48–54.
[8] M. Wei, Y. Qiao, H. Zhao, J. Liang, T. Li, Y. Luo, S. Lu, X. Shi, W. Lu, X. Sun, Electrochemical non-enzymatic glucose sensors: recent progress and perspectives, Chem. Commun. 56 (2020) 14553–14569.
[9] R. Ahmad, M. Vaseem, N. Tripathy, Y.-B. Hahn, Wide linear-range detecting nonenzymatic glucose biosensor based on CuO nanoparticles inkjet-printed on electrodes, Anal. Chem. 85 (2013) 10448–10454.
[10] F. Franceschini, I. Taurino, Nickel-based catalysts for non-enzymatic electrochemical sensing of glucose: a review, Phys. Med. 14 (2022), 100054.
[11] A. Sanati, Y. Esmaeili, E. Bidram, L. Shariati, M. Rafienia, S. Mahshid, O. Parlak, Recent advancement in electrode materials and fabrication, microfluidic designs, and self-powered systems for wearable non-invasive electrochemical glucose monitoring, Appl. Mater. Today 26 (2022), 101350.
[12] Q. Dong, H. Ryu, Y. Lei, Metal oxide based non-enzymatic electrochemical sensors for glucose detection, Electrochim. Acta 370 (2021), 137744.
[13] E. Sehit, Z. Altintas, Significance of nanomaterials in electrochemical glucose sensors: An updated review (2016-2020), Biosens. Bioelectron. 159 (2020), 112165.
[14] M.M. Alam, M.M.R. Howlader, Nonenzymatic electrochemical sensors via Cu native oxides (CuNOx) for sweat glucose monitoring, Sensing and Bio-Sensing Res. 34 (2021), 100453.
[15] I.M. Tiginyanu, O. Lupan, V.V. Ursaki, L. Chow, M. Enachi, 3.11 - Nanostructures of Metal Oxides, in: P. Bhattacharya, R. Fornari, H. Kamimura (Eds.) Comprehensive Semiconductor Science and Technology, Elsevier, Amsterdam, 2011, pp. 396–479.
[16] D. Nunes, A. Pimentel, L. Santos, P. Barquinha, L. Pereira, E. Fortunato, R. Martins, 3 - Structural, optical, and electronic properties of metal oxide nanostructures, in: D. Nunes, A. Pimentel, L. Santos, P. Barquinha, L. Pereira, E. Fortunato, R. Martins (Eds.), Metal Oxide Nanostructures, Elsevier, 2019, pp. 59–102.
[17] A.-J. Wang, J.-J. Feng, Z.-H. Li, Q.-C. Liao, Z.-Z. Wang, J.-R. Chen, Solvothermal synthesis of Cu/Cu2O hollow microspheres for non-enzymatic amperometric glucose sensing, CrystEngComm 14 (2012) 1289–1295.
[18] L. Zhang, H. Li, Y. Ni, J. Li, K. Liao, G. Zhao, Porous cuprous oxide microcubes for non-enzymatic amperometric hydrogen peroxide and glucose sensing, Electrochem. Commun. 11 (2009) 812–815.
[19] M.-M. Guo, Y. Xia, W. Huang, Z. Li, Electrochemical fabrication of stalactite-like copper micropillar arrays via surface rebuilding for ultrasensitive nonenzymatic sensing of glucose, Electrochim. Acta 151 (2015) 340–346.

[20] S. Liu, J. Tian, L. Wang, X. Qin, Y. Zhang, Y. Luo, A.M. Asiri, A.O. Al-Youbi, X. Sun, A simple route for preparation of highly stable CuO nanoparticles for nonenzymatic glucose detection, Catal. Sci. Technol. 2 (2012) 813–817.
[21] X. Liu, W. Yang, L. Chen, J. Jia, Synthesis of copper nanorods for non-enzymatic amperometric sensing of glucose, Microchim. Acta 183 (2016) 2369–2375.
[22] Y. Zhang, Y. Liu, L. Su, Z. Zhang, D. Huo, C. Hou, Y. Lei, CuO nanowires based sensitive and selective non-enzymatic glucose detection, Sens. Actuators B: Chem. 191 (2014) 86–93.
[23] Z. Zhuang, X. Su, H. Yuan, Q. Sun, D. Xiao, M.M.F. Choi, An improved sensitivity non-enzymatic glucose sensor based on a CuO nanowire modified Cu electrode, Analyst 133 (2008) 126–132.
[24] W. Wang, L. Zhang, S. Tong, X. Li, W. Song, Three-dimensional network films of electrospun copper oxide nanofibers for glucose determination, Biosens. Bioelectron. 25 (2009) 708–714.
[25] Z. Gao, J. Liu, J. Chang, D. Wu, J. He, K. Wang, F. Xu, K. Jiang, Mesocrystalline Cu2O hollow nanocubes: synthesis and application in non-enzymatic amperometric detection of hydrogen peroxide and glucose, CrystEngComm 14 (2012) 6639–6646.
[26] H. Cao, A. Yang, H. Li, L. Wang, S. Li, J. Kong, X. Bao, R. Yang, A non-enzymatic glucose sensing based on hollow cuprous oxide nanospheres in a Nafion matrix, Sens. Actuators B: Chem. 214 (2015) 169–173.
[27] S. Cherevko, C.-H. Chung, The porous CuO electrode fabricated by hydrogen bubble evolution and its application to highly sensitive non-enzymatic glucose detection, Talanta 80 (2010) 1371–1377.
[28] M.U. Anu Prathap, B. Kaur, R. Srivastava, Hydrothermal synthesis of CuO micro-/nanostructures and their applications in the oxidative degradation of methylene blue and non-enzymatic sensing of glucose/H2O2, J. Colloid Interface Sci. 370 (2012) 144–154.
[29] S. Wang, M. Zheng, X. Zhang, M. Zhuo, Q. Zhou, Y. Su, M. Zheng, G. Yuan, Z. Wang, Flowerlike CuO/Au nanoparticle heterostructures for nonenzymatic glucose detection, ACS Appl. Nano Mater. 4 (2021) 5808–5815.
[30] N. Theaker, J.M. Strain, B. Kumar, J.P. Brian, S. Kumari, J.M. Spurgeon, Heterogeneously catalyzed two-step cascade electrochemical reduction of CO_2 to ethanol, Electrochim. Acta 274 (2018) 1–8.
[31] C.W. Li, M.W. Kanan, CO_2 Reduction at Low Overpotential on Cu electrodes resulting from the reduction of thick Cu2O films, J. Am. Chem. Soc. 134 (2012) 7231–7234.
[32] C.W. Li, J. Ciston, M.W. Kanan, Electroreduction of carbon monoxide to liquid fuel on oxide-derived nanocrystalline copper, Nature 508 (2014) 504–507.
[33] Y.H. Won, L.A. Stanciu, Cu2O and Au/Cu2O particles: surface properties and applications in glucose sensing, Sensors 12 (2012) 13019–13033.
[34] A. Kusior, Voltammetric detection of glucose-the electrochemical behavior of the copper oxide materials with well-defined facets, Sensors 22 (2022).
[35] C.-H. Kuo, Y.-C. Yang, S. Gwo, M.H. Huang, Facet-dependent and Au nanocrystal-enhanced electrical and photocatalytic properties of Au−Cu2O core−shell heterostructures, J. Am. Chem. Soc. 133 (2011) 1052–1057.
[36] S. Felix, P. Kollu, B.P.C. Raghupathy, S. Kwan Jeong, A. Nirmala Grace, Electrocatalytic activity of Cu2O nanocubes based electrode for glucose oxidation, J. Chem. Sci. 126 (2014) 25–32.
[37] X. Xiao, J. Ulstrup, H. Li, Me Wang, J. Zhang, P. Si, Nanoporous gold assembly of glucose oxidase for electrochemical biosensing, Electrochim. Acta 130 (2014) 559–567.
[38] C. Dong, H. Zhong, T. Kou, J. Frenzel, G. Eggeler, Z. Zhang, Three-dimensional Cu foam-supported single crystalline mesoporous Cu2O nanothorn arrays for ultra-highly sensitive and efficient nonenzymatic detection of glucose, ACS Appl. Mater. Interfaces 7 (2015) 20215–20223.
[39] B. Barbee, B. Muchharla, A. Adedeji, A. Karoui, K. Kumar Sadasivuni, M.S. Sha, A. M. Abdullah, G. Slaughter, B. Kumar, Cu and Ni Co-sputtered heteroatomic thin film for enhanced nonenzymatic glucose detection, Sci. Rep. 12 (2022) 7507.
[40] G. Liu, J. Zhao, L. Qin, S. Liu, Q. Zhang, J. Li, Synthesis of an ordered nanoporous Cu/Ni/Au film for sensitive non-enzymatic glucose sensing, RSC Adv. 10 (2020) 12883–12890.
[41] Y. Zhang, L. Su, D. Manuzzi, H.V.E. de los Monteros, W. Jia, D. Huo, C. Hou, Y. Lei, Ultrasensitive and selective non-enzymatic glucose detection using copper nanowires, Biosens. Bioelectron. 31 (2012) 426–432.
[42] P. Viswanathan, J. Park, D.-K. Kang, J.-D. Hong, Polydopamine-wrapped Cu/Cu(II) nano-heterostructures: an efficient electrocatalyst for non-enzymatic glucose detection, Colloids Surf. A: Physicochem. Eng. Asp. 580 (2019), 123689.
[43] R. Li, X. Liu, H. Wang, Y. Wu, K.C. Chan, Z. Lu, Sandwich nanoporous framework decorated with vertical CuO nanowire arrays for electrochemical glucose sensing, Electrochim. Acta 299 (2019) 470–478.
[44] R. Ahmad, M. Khan, P. Mishra, N. Jahan, M.A. Ahsan, I. Ahmad, M.R. Khan, Y. Watanabe, M.A. Syed, H. Furukawa, A. Khosla, Engineered hierarchical CuO nanoleaves based electrochemical nonenzymatic biosensor for glucose detection, J. Electrochem. Soc. 168 (2021), 017501.
[45] V. Vinoth, T.D. Shergilin, A.M. Asiri, J.J. Wu, S. Anandan, Facile synthesis of copper oxide microflowers for nonenzymatic glucose sensor applications, Mater. Sci. Semicond. Process. 82 (2018) 31–38.
[46] K. Li, G. Fan, L. Yang, F. Li, Novel ultrasensitive non-enzymatic glucose sensors based on controlled flower-like CuO hierarchical films, Sens. Actuators B: Chem. 199 (2014) 175–182.
[47] H.-H. Fan, W.-L. Weng, C.-Y. Lee, C.-N. Liao, Electrochemical cycling-induced spiky CuxO/Cu nanowire array for glucose sensing, ACS Omega 4 (2019) 12222–12229.
[48] J. Lv, C. Kong, Y. Xu, Z. Yang, X. Zhang, S. Yang, G. Meng, J. Bi, J. Li, S. Yang, Facile synthesis of novel CuO/Cu2O nanosheets on copper foil for high sensitive nonenzymatic glucose biosensor, Sens. Actuators B: Chem. 248 (2017) 630–638.
[49] V.V. Khedekar, B.M. Bhanage, Simple electrochemical synthesis of cuprous oxide nanoparticles and their application as a non-enzymatic glucose sensor, J. Electrochem. Soc. 163 (2016) B248.
[50] Y. Ao, J. Ao, L. Zhao, L. Hu, F. Qu, B. Guo, X. Liu, Hierarchical structures composed of Cu(OH)2 nanograss within directional microporous Cu for glucose sensing, Langmuir 38 (2022) 13659–13667.